www.trjfas.org
ISSN 1303-2712
Turkish Journal of Fisheries and Aquatic Sciences 18: 705-716 (2018) DOI: 10.4194/1303-2712-v18_5_06

RESEARCH PAPER

Numerical Study on the Flow Field Around a Fish Farm in Tidal Current

Chun-Wei Bi[1], Tiao-Jian Xu[1,*]

[1] Dalian University of Technology, State Key Laboratory of Coastal and Offshore Engineering, Dalian 116024, China.

* Corresponding Author: Tel.: +86.411 84708300; Fax: +86.411 84671713;
E-mail: tjxu@dlut.edu.cn

Received 12 July 2017
Accepted 18 September 2017

Abstract

The netting of the fish farm, with biofouling or not, was simulated using the porous-media fluid model. The porous coefficients for both clean and biofouled netting were calculated from the drag and lift forces that acts on corresponding clean or biofouled plane net, consequently the relationship between the porous coefficients and the features of the netting as well as the biofouling is established. In this study, both constant and tidal currents through a fish farm, consisting of 2×4 full-scale net cages, were investigated numerically. Effects of cage height, incidence angle of the current and level of biofouling on the netting on the flow field in vicinity region of the fish farm were presented and discussed. Compared with constant current, tidal current produces different flow pattern downstream from the fish farm. Overall, the height of the wake region downstream from the fish farm increases with increasing cage height. The attenuation in flow velocity both inside the net cage and in the wake region increases as the level of biofouling increases. With respect to the incidence angle of the tidal current, the optimal orientation of the fish farm can be determined in certain tidal current from an ecological perspective.

Keywords: Net cage, biofouling, tidal current, flow field, numerical simulation.

Introduction

China has become the biggest exporter of aquatic product in the world owing to the rapid expansion in its fish production particularly from aquaculture (FAO, 2014). To ensure a steady supply of aquatic products, efforts must be paid to aquaculture in fish farm. The environmental conditions inside and around the fish farm are important for the welfare and development of the fish. The optimal locality for fish farming should provide optimal water quality for the caged fish, ensure sufficient water exchange through the fish farm and minimize environmental impacts, such as the erosion of the bottom sediment. Therefore, shifting the aquaculture in fish farm from inner bay to offshore is becoming inevitable trends. When deployed in offshore, the fish farm tends to be exposed to the tidal current instead of the constant current (Cornejo, Sepúlveda, Gutiérrez, & Olivares, 2014; Wu *et al*., 2014; Xu, Hou, Dong, Zhao, & Guo, 2017). Thus, the study on tidal currents through the net cages is of great importance.

Similar to other marine structures, the netting of the net cage in fish farm suffers from the effects of biofouling in the open sea (Figure 1). Biofouling, the accumulation of marine organisms, is prone to leading to rapid occlusion of the netting mesh (Braithwaite, Carrascosa, & McEvoy, 2007), which may causes the following disadvantages: i) biofouling communities acting as disease reservoirs can increase disease risk to the farmed fish (Fitridge, Dempster, Guenther, & de Nys, 2012), ii) the hydrodynamic forces acting on the net cage are dramatically increased, which increases the risk of structural failure and fatigue damage of the net cage (Klebert, Lader, Gansel, & Oppedal, 2013), iii) the biofouled netting is easily deformed in currents and thus causes negative effect on the effective volume for the farmed fish and iv) the attenuation of currents through the net cage is increased, which decreases the water exchange and oxygen supply inside the net cage. The water flow inside and around the fish farm is critical for efficient and sustainable aquaculture production. Thus, the investigation on flow through a fish farm in tidal current has great significance for aquaculture.

A large number of researches have been worked on determining the flow field inside and around the net cages. Aarsnes, Rudi, and Løland (1990) conducted a series of physical-model experiments to investigate the flow velocity in net cages as well as the drag force and the deformation of the netting. Johansson, Juell, Oppedal, Stiansen, and Ruohonen

Figure 1. Images of the biofouled nettings of the net cage in fish farm.

(2007) found 33~64% attenuation in flow velocity by field measurements at four fish farms. Harendza, Visscher, Gansel, and Pettersen (2008) conducted laboratory experiments with PIV (particle image velocimetry) technique to study flow through the net-cage models at varioius inclination angles. Rasmussen, Patursson, and Simonsen (2015) studied the wake structure of a fish farm in tidal current using the acoustic doppler current profiler (ADCP) and the minimum water exchange velocity was found. Among the numerical works, Shim, Klebert, and Fredheim (2009) presented the flow field inside and behind a net cage with various porosities using the porous-jump media model. Zhao *et al*. (2013) proposed a numerical model based on a porous-media fluid model and the flow fields around tandem net cages were simulated. Cornejo *et al*. (2014) numerically studied the flow-velocity distribution downstream from a salmon farm in semidiurnal current. Chen and Christensen (2016) developed a numerical model based on OpenFOAM to study steady current flow through plane net panels and circular fish cages.

While, the above studies relate to flow through the net cage or fish farm, there is paucity of research taking the biofouling problem into account. Swift *et al*. (2006) carried out field measurements with 1m×1m plane nets accumulated by various amounts of biofouling and the drag force acting on the biofouled netting was discussed. Gansel, McClimans, and Myrhaug (2012) conducted physical-model tests on six cylindrical nettings using PIV technique to study the average flow fields around net cages with an attempt to analyze the biofouling effect. Gansel *et al*. (2015) measured drag forces on both clean and biofouled nettings in laboratory experiment and the relationship between net solidity and drag was assessed. Lader *et al*. (2015) performed field tests to investigate the growth characteristics of hydroids growing on a net and conducted laboratory experiments to study the hydrodynamic drag on the fouled twines by using fabricated models of net twines with artificial hydroid fouling. Through the review of literature, there is paucity of dedicated and conclusive study on the flow field around the biofouled netting. Hence this study aims to investigate the flow field around a fish farm consisting of 2×4 full-scale net cages. Three scenarios were considered: (i) net cages with various heights in both tidal and constant currents; (ii) net cages with various levels of biofouling in a semi-diurnal current and (iii) biofouled net cages in various incidence angles in a semi-diurnal current.

Description of Numerical Model

In this study, a three-dimensional numerical flume was built mainly based on the Navier-Stokes equations with the capacity to generate constant current, semi-diurnal and diurnal tides. Both the clean and biofouled netting of the net cage were simulated using the porous-media fluid model. Described by the same set of governing equations, the net-cage model and the numerical flume can be coupled.

Governing equations review

In the present numerical model, the governing equations comprises the Navier-Stokes equations coupled with the realizable k–ε model, which have been described in details in our previous studies (Bi, Zhao, & Dong, 2015; Zhao *et al*., 2013), thus a brief review is given here. Navier-Stokes equation are

$$\rho\frac{\partial u_i}{\partial x_i}=0 \tag{1}$$

$$\rho\frac{\partial u_i}{\partial t}+\rho\frac{\partial\left(u_iu_j\right)}{\partial x_j}=-\frac{\partial P}{\partial x_i}+\rho g_i+\frac{\partial}{\partial x_j}\left(\mu+\mu_t\right)\left(\frac{\partial u_i}{\partial x_j}+\frac{\partial u_j}{\partial x_i}\right)+S_i \tag{2}$$

where t is time; μ is the viscosity; ρ is the density of water; μ_t is the eddy viscosity; $P=p+\left(2/3\right)\rho k$, where p represents pressure; k represents the turbulent kinetic energy; u_i and u_j are the average velocity component, respectively; g_i is the gravity acceleration; i, j=1, 2, 3 (x, y, z); and S_i is an additional item for the description of both clean and biofouled netting.

The realizable k–ε model (Shih, Liou, Shabbir, Yang, & Zhu, 1995) is introduced to close the equations, where k equation is

$$\rho\frac{\partial k}{\partial t}+\rho\frac{\partial(ku_i)}{\partial x_i}=\frac{\partial}{\partial x_j}\left[\left(\mu+\frac{\mu_t}{\sigma_k}\right)\frac{\partial k}{\partial x_j}\right]+G_k+G_b-\rho\varepsilon-Y_M+S_k \tag{3}$$

and ε equation is given by

$$\rho\frac{\partial(\varepsilon u_i)}{\partial x_i}=\frac{\partial}{\partial x_j}\left[\left(\mu+\frac{\mu_t}{\sigma_\varepsilon}\right)\frac{\partial\varepsilon}{\partial x_j}\right]+\rho C_1S\varepsilon-\rho C_2\frac{\varepsilon^2}{k+\sqrt{\nu\varepsilon}}+C_{1\varepsilon}\frac{\varepsilon}{k}C_{3\varepsilon}G_b+S_\varepsilon \tag{4}$$

$$C_1=\max\left[0.43,\frac{\eta}{\eta+5}\right],\quad \eta=S\frac{k}{\varepsilon},\quad S=\sqrt{2S_{ij}S_{ij}},\quad S_{ij}=\frac{1}{2}\left(\frac{\partial u_i}{\partial x_j}+\frac{\partial u_j}{\partial x_i}\right) \tag{5}$$

In the equations, G_k is the turbulent kinetic energy generated by the average velocity gradient. G_b and Y_M due to buoyancy and compressibility are not necessary when modeling incompressible fluid with no temperature fluctuations, hence $G_b = 0$ and $Y_M = 0$. C_2, $C_{1\varepsilon}$ and $C_{3\varepsilon}$ are constants; S is the modulus of the mean rate-of-strain tensor; σ_k and σ_ε are the turbulent Prandtl number; and S_k and S_ε are user defined source terms. The model constants are $C_{1\varepsilon} = 1.44$, $C_2 = 1.9$, $\sigma_k = 1.0$ and $\sigma_\varepsilon = 1.2$ for the realizable k–ε turbulence model (Shih *et al*., 1995).

The governing equations are solved using commercial code ANSYS FLUENT 15.0 where the finite volume method (FVM) is adopt for discretization. The pressure interpolation and momentum equation are discretized using second-order upwind scheme. The iteration of coupling between pressure and velocity uses the SIMPLEC (Semi-implicit Method for Pressure-linked Equations-consistent) algorithm. In this study, the time step is set to 200 s for the time discretization.

Net-cage model considering biofouling effect

A typical net cage comprises the float collar, sinkers, mooring system and the netting which forms the main space for aquaculture. As the most part of the float collar is above the free surface of the water and the sinkers and mooring system are relatively small-scale components. Thus, only the netting is simulated in this numerical model and the cylindrical netting is divided into 16 plane nets around the circumference and one bottom net (Bi *et al*., 2015). Both the clean and biofouled netting of the net cage were simulated using the porous-media fluid model and the corresponding porous coefficients were determined from the hydrodynamic forces acting on the plane-net sheet which are correlated with the features of the biofouled netting (Bi *et al*., 2015; Zhao *et al*., 2013).

The porous-media fluid model is a hypothetical model that acts in the same way as the water-blocking effect for both clean and biofouled netting by setting the porous coefficients. Inside the porous media, S_i is calculated by the following equation:

$$S_i=-C_{ij}\frac{1}{2}\rho|\vec{u}|\vec{u} \tag{6}$$

where C_{ij} is given by

$$C_{ij}=\begin{pmatrix} C_n & 0 & 0\\ 0 & C_t & 0\\ 0 & 0 & C_t\end{pmatrix} \tag{7}$$

where C_{ij} is porous-coefficient matrices, C_n is the normal-resistance coefficient, and C_t is the tangential-resistance coefficient. The source term for the momentum equation is zero outside the porous media. It should be noted that the unit of the porous coefficient is m^{-1}. The calculation process of the porous coefficients for the net-cage model is listed in Appendix A.

Numerical flume and boundary conditions

The coordinate system for the numerical model is set as follows: x is positive along the flow direction, y is perpendicular to the flow direction on the horizontal plane and z is upward (Figure 2). The dimensions of the numerical flume are 2000 m long, 1000 m wide and 50 m depth. The computational domain is discretized with structured grid with a resolution of 1~5 m inside and in the vicinity of the fish farm.

Both the upstream and downstream boundaries of the numerical flume are described by the velocity inlet which produce currents in opposite directions. The flow velocity of the semi-diurnal current is imposed using UDF (user defined function) as the following formula:

$$u=u_m\sin(2\pi\frac{t}{T}) \tag{8}$$

where u_m is the maximum velocity and T is the

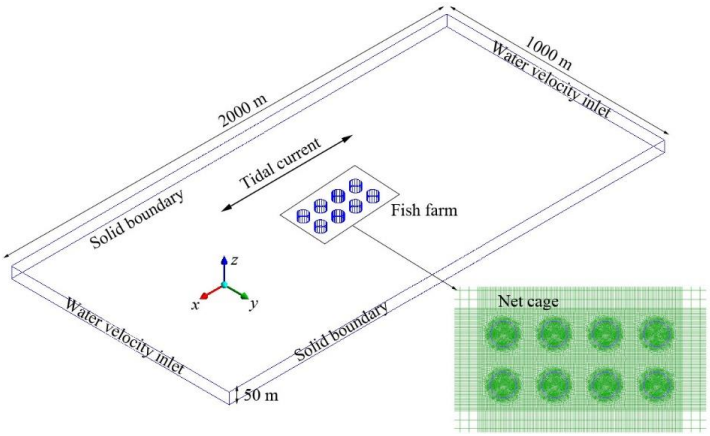

Figure 2. Computational domain of the numerical model and computational mesh around the net cages.

period of the semi-diurnal current which is 12 h. The water level is modeled using zero-shear-stress wall without rise and fall, where two facts are considered: i) the net cage is prone to floating on the free surface and ii) the alternating current induces limited variation in water depth with a low current velocity. The bottom of the numerical model is defined as no-slip-wall and the wall function is adopt to simulate the viscous of the fluid near the surface. The lateral boundary conditions of the numerical flume are described by zero-shear-stress wall boundaries.

Numerical Simulations

Tidal currents through a fish farm, comprising 2×4 full-scale circular net cages with a diameter (D) of 40 m and a depth (H) of 25 m, are simulated. The center-to-center spacing is 80 m (equal to 2D) between two neighboring net cages. The flow fields in the vicinity of the fish farm are discussed with different cage heights, incidence angles of the current and levels of biofouling on the netting.

Numerical model description

Both tidal and constant currents through the fish farm with the incidence angle of 0° was investigated numerically with different cage heights: H/h_0=0.1, 0.3, 0.5, 0.7 and 0.9. Besides, tidal currents through the fish farm at 0° were modeled with different levels of biofouling. Table 1 shows the porous coefficients for the netting model with a thickness of 1 m corresponding to both clean and biofouled nettings. The porous coefficients were mainly determined by the field measurements of Swift *et al*. (2006) together with the empirical formulas by Aarsnes *et al*. (1990), which has been described in details in our previous work (Bi *et al*., 2015). To analyze the effect of incidence angle on the flow field, tidal currents through the fish farm at 0°, 22.5°, 45°, 67.5° and 90° were investigated numerically without considering the effect of biofouling. All the numerical simulations were performed in a semi-diurnal current for a maximum velocity of 0.1 m s^{-1} which is considered as a low current velocity (Johansson *et al*., 2014). The water depth (h_0) is 50 m.

Results and Discussion

Effect of Cage Height

Figure 3a presents the tidal current fields inside and around the fish farm with different cage heights in the ebb tide with a free stream velocity of 0.1 m s^{-1}. As the net cages cover more and more water column, the height of the wake region downstream from the fish farm increases with increasing cage height. However, there is no significant variation in the length of the wake for different cage heights. In contrast, the length of wake increases and the flow-velocity-reduction region shifts downstream progressively with increasing cage height in constant current at 0.1 m s^{-1} (Figure 3b).

Due to the blockage of the netting, the flow velocity continuously decreases in the flow direction till the downstream boundary of the fish farm with different cage heights in both tidal and constant currents (Figure 4). Then, the flow velocity starts to increase in the wake of the fish farm which is attribute to the fluid recovery mechanism. Overall, the flow velocity inside the fish farm is insensitive to the cage height in different conditions. For flow velocity downstream from the fish farm, the variation trend shows no significant difference for different cage heights and the maximum reduction is ranging from 35.5% to 39.0% in tidal current. In contrast, the flow velocity decreases progressively as the cage height increases in constant current. The maximum attenuation in flow velocity from 35.7% to 46.9% can be found in the wake of the fish farm. For cage height H/h_0=0.1, there is noticeable fluctuation in flow velocity inside the downstream net cages which may negatively impact the welfare of the fish.

The numerical results of flow velocity through the fish farm in constant current are compared with the results from formulas derived by Løland (Aarsnes *et al*., 1990) (Figure 4b). The formulas, based on theoretical work combined with experimental data, are as follows:

$$u = u_0 \prod_{i=1}^{n_c} r_i \tag{9}$$

where r_i is the flow velocity reduction factor which is given by

$$r_i = 1.0 - 0.46 C_d \tag{10}$$

where n_c is the number of netting for water flow through and C_d is 0.175 for the netting without biofouling as shown in Table 1. The results show a good agreement between the present model and Løland's formula at various positions in the fish farm.

Table 1 Drag coefficients of the nettings and corresponding porous coefficients for different numerical cases

Case no.	Solidity	Biofouling level	C_d	C_n (m^{-1})	C_t (m^{-1})
1	0.121	No fouling	0.175	0.197	0.127
2	0.547	Light	0.260	0.307	0.198
3	0.502	Medium	0.318	0.388	0.250
4	0.743	Heavy	0.513	0.708	0.457
5	0.566	Extremely heavy	0.599	0.881	0.568

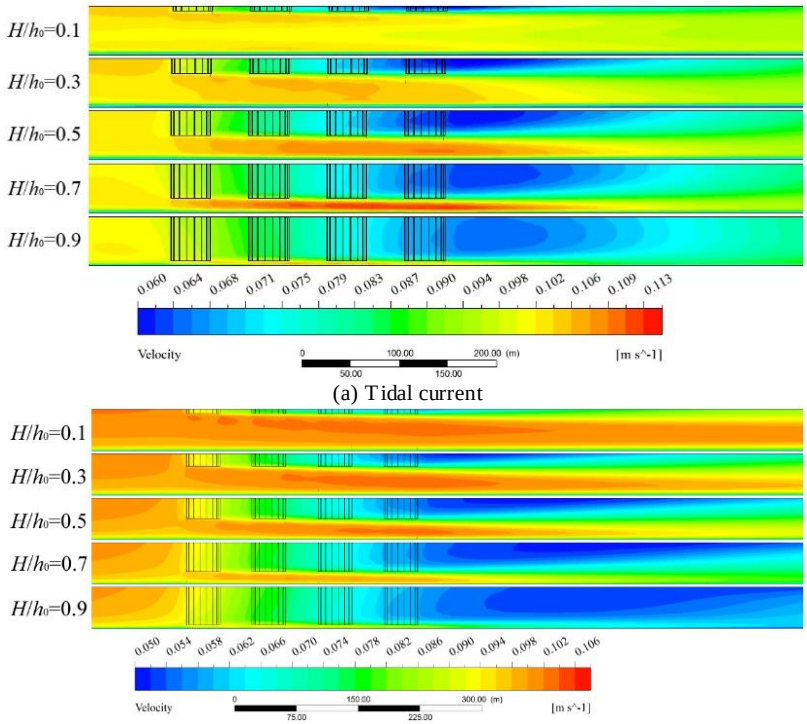

(a) Tidal current

(b) Constant current

Figure 3. Numerical results of flow fields within and around net cages with different cage heights on the vertical plane through the cage center.

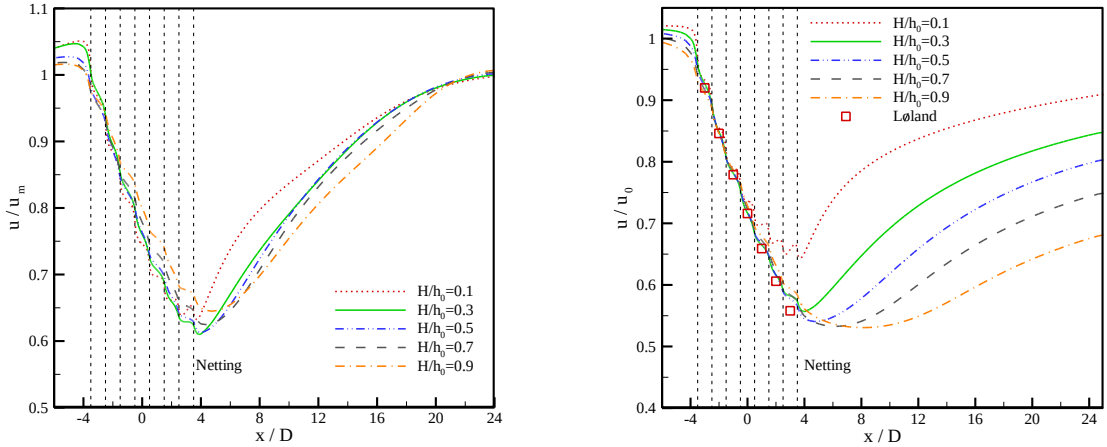

(a) Tidal current

(b) Constant current

Figure 4. Numerical results of flow velocity along the horizontal centerline of the net cages with different cage heights.

This provides confidence that the proposed numerical model can simulate the flow field inside and around the fish farm accurately.

Using the proposed numerical model, this study also compares the non-dimensional flow velocity downstream from the fish farm in constant current, semi-diurnal and diurnal tides with the same intensity (Table 2). The flow-velocity reduction in constant current was very large, followed by diurnal tide, and semi-diurnal tide had the least effect. Thus, the flow pattern around the fish farm can be different in different current conditions.

The vertical distributions of the tidal velocity are shown in Figure 5, which are strongly sensitive to the variation in cage height. As expected, there is noticeable attenuation in flow velocity inside the downstream net cages with different cage heights. Due to mass conservation, the flow velocity progressively increases along the water depth and then decreases after reaching the peak value. The numerical results indicate that the net cage with the height of H/h_0=0.7 produces the maximal peak value of flow velocity beneath the fish farm. When the cage height reaches H/h_0=0.9, the attenuation in flow velocity in the net cage is lower than that with other cage heights and marginally increase in flow velocity

is observed beneath the net cage. This means that an increase in the cage height plays an important role in the flow velocity beneath the fish farm which is associated with the erosion of the seabed sediment (Wu *et al*., 2014).

Effect of Biofouling on Fishing Net

Figure 6 shows the Eulerian record of tidal velocity at the center of the most downstream net cages. In all cases, the flow velocity inside the net cage vary periodically corresponding to the tidal current. After the first period, the flow velocity increases marginally in the time domain, which is due to the effect of positive wake (i.e. a high velocity area upstream of the fish farm, defined by Cornejo *et al*. (2014)). The attenuation in flow velocity is pronounced, approximately 40%~60%, in the positive tidal current as water passes through seven layers of netting before reaches the monitored point. However, much less reduction is observed during the inversion of current direction because water passes through only one layer of netting which produces much less blockage.

To show horizontal changes in flow field under tidal current, flow-velocity distributions within and around the net cages are plotted in the ebb tide with a free stream velocity of 0.1 m s^{-1}. Figure 7 shows the

Table 2 Non-dimensional flow velocity u/u_m downstream from the fish farm in different current conditions.

Current condition	u/u_m
Semi-diurnal tide	0.669
Diurnal tide	0.569
Constant current	0.541

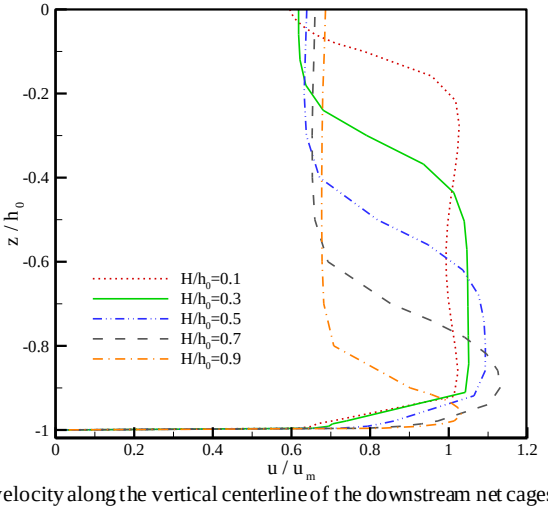

Figure 5. Numerical results of flow velocity along the vertical centerline of the downstream net cages with different cage heights.

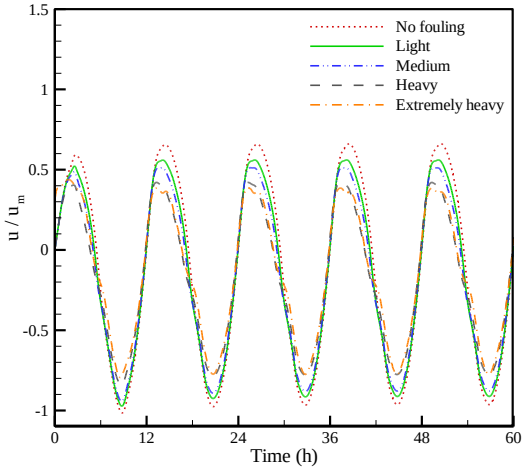

Figure 6. Time-series comparisons of tidal velocity at the center of the downstream net cages with different levels of biofouling.

flow field on the horizontal plane 12.5 m below the water surface which is considered to represent the flow pattern around the net cages. There are noticeable flow-velocity reductions within and downstream from the net cages at various levels of biofouling. Overall, the attenuation in flow velocity both inside the net cage and in the wake region increases as the level of biofouling increases. In contrast, the flow velocity increases between two rows of net cages and at the flanks due to mass conservation (Kristiansen & Faltinsen, 2012), resulting from the presence of the net cages. The maximum flow velocity could be raised by approximately 23% between two rows of net cages, while it is approximately 13% at the flanks of the fish farm. Overall, the higher the amount of biofouling, the greater the effect on the flow field (Figure 8).

A non-dimensional flow velocity u/u_m is introduced to describe the variation in tidal current field which is defined as the ratio of a local flow velocity to the free-stream velocity. As flow through the biofouled netting, the flow velocity continuously decreases in the region of fish farm but then increases in the wake of the fish farm at various levels of biofouling (Figure 9). The flow-velocity reduction region (wake) extends for approximately 20 times of cage diameter downstream from the fish farm in all cases. It is intuitive that larger current velocity causes

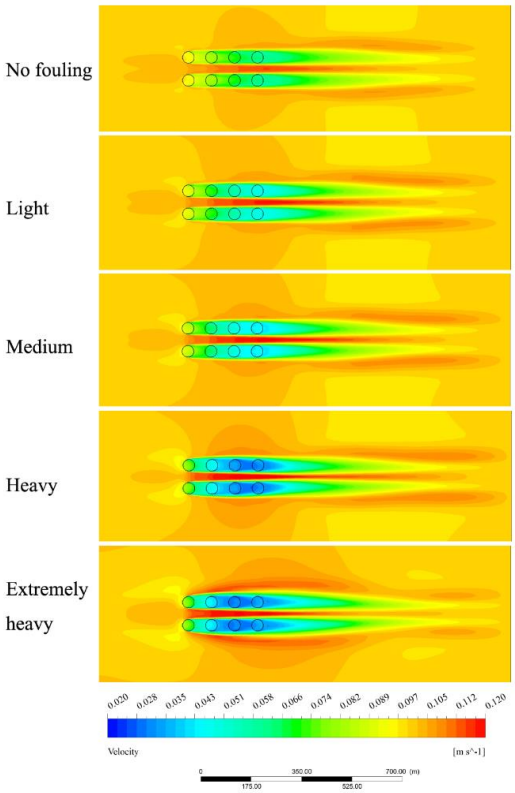

Figure 7. Numerical results of flow fields within and around net cages with different levels of biofouling on the horizontal plane 12.5 m below the water surface.

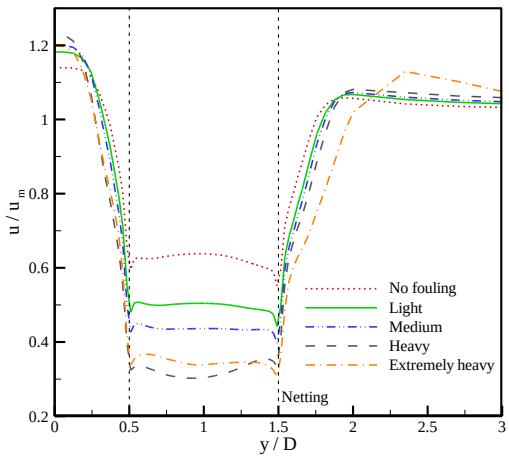

Figure 8. Numerical results of flow velocity along the lateral centerline of the downstream net cages with different levels of biofouling.

larger wake (Cornejo *et al*., 2014). Besides, the net solidity and the number of the net cage in the fish farm are also considered to be factors affecting wake formation, which will be further studied in future. For the clean net cages, the maximum attenuation in flow velocity is 38.3% which is monitored at approximately equal to the cage diameter downstream from the center of the downstream net cage. In contrast, as the level of biofouling increases, the maximum attenuation in flow velocity from 51.0% to 70.1% can be found in the vicinity of the downstream net cage. However, the variation of the flow velocity in the fish farm are very similar for cases 4 and 5. It suggests that the flow velocity will not consistently decrease with increasing level of biofouling. As flow through the clean net cage is also presented, the sole effect of the biofouling on the flow field can be derived by subtracting the effect of the clean net cage from that of a biofouled one.

Effect of Incidence Angle of the Current

The tidal current fields inside and around the fish farm in the ebb tide with a free stream velocity of 0.1

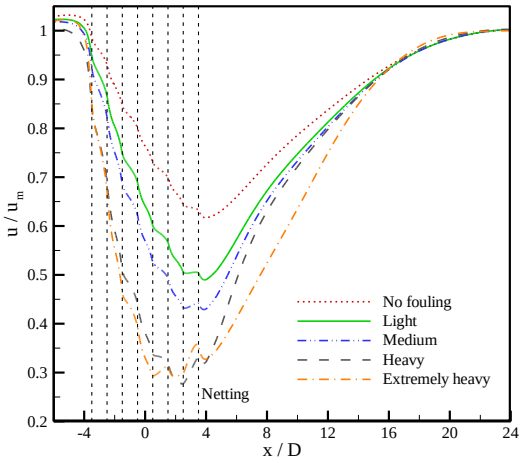

Figure 9. Numerical results of flow velocity along the horizontal centerline of the net cages with different levels of biofouling.

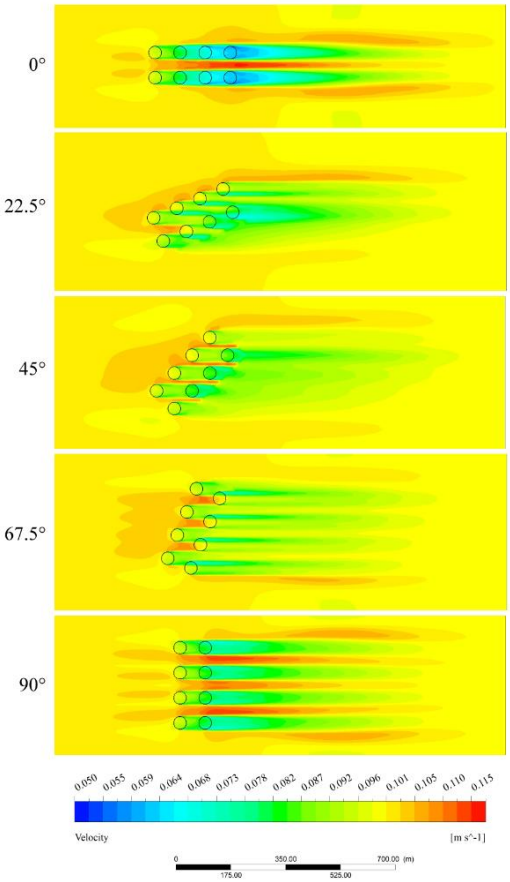

Figure 10. Numerical results of flow fields within and around the fish farm with different incidence angles on the horizontal plane 12.5 m below the water surface.

m s^{-1} are shown in Figure 10. The numerical result indicates that the incidence angle of the tidal current can affect the flow fields within and around the net cages significantly. As the incidence angle increases, the positive-wake region upstream the fish farm is prone to increase, while the attenuation in flow velocity downstream from the fish farm tends to decrease. Compared with the tandem net cages, the staggered ones present more noticeable blockage effect on incoming flow, which results in an uniformly distributed wake downstream from the fish farm. When the incidence angle reaches 90°, the tidal current produce similar flow pattern around the fish farm with that of 0°, because the net cages become tandem again. As expected, the attenuation in flow velocity downstream from the fish farm at 90° is smaller than that at 0° because of less tandem net cage in the flow direction (Figure 11). For 0° incidence angle, the flow velocity is attenuated by approximately 37.1% in the wake, while it is increased between two rows of net cages by 14.4% and at the flanks by 5.4% due to mass conservation. In contrast, the flow field shows the least variation in flow velocity downstream the fish farm with the incidence angle of 45°, which indicates the minimal impact on the environment.

The flow velocity at the center of the net cage is monitored to present the flow field inside a net cage among the fish farm (Figure 12). Among the five incidence angles, the non-dimensional flow velocity u/u_m inside the net cage is ranging from 0.64 to 1.03. Inside most of the net cages, noticeable attenuation in flow velocity exists due to the blockage effect (or shadowing effect) of the netting. However, there is no reduction even has slightly increase in flow velocity inside some downstream net cages, because of the interaction between the wakes from different neighboring net cages. For the incidence angle of 67.5°, relatively larger flow velocities (0.96~1.03) are monitored inside the net cages, which is considered to be beneficial to the water exchange. Moreover, flow velocities are similar inside all the cages of the fish farm, which indicates that the incidence angle of 67.5° has advantage in providing a uniform flow environment for the caged fish. On this basis, the optimal orientation of the fish farm can be determined in certain tidal current from an ecological perspective.

As current flows through net cages in a fish farm, especially when considering the biofouling on the net, the flow velocity is attenuated in the vicinity region due to the shielding effect of the netting. Thus, the hydrodynamic loads acting on and the water exchange of the net cage will be changed correspondingly. Besides, the investigation on the flow field downstream from the fish farm has implication for integrated multi-trophic aquaculture (IMTA, shown in Figure 13) configurations which consist of finfish cages, inorganic extractive species (such as kelp) and organic extractive species (such as shellfish). The flow field downstream from the finfish cage is essential to predict the transport of dissolved nutrients and the hydrodynamic performance of IMTA.

Conclusions

The study investigated tidal current through a fish farm consisting of 2×4 full-scale net cages with numerical approach. The flow-velocity distributions within and around the net cages are discussed with different cage heights, incidence angles of the current and levels of biofouling on the netting. Below are the main conclusions:

(i) The height of the wake region downstream from the fish farm increases with increasing cage height. The net cage with the non-dimensional height of H/h_0=0.7 produces the maximal peak value of flow velocity beneath the fish farm. Different flow patterns are observed in different current conditions. The flow-velocity reduction in constant current was very large,

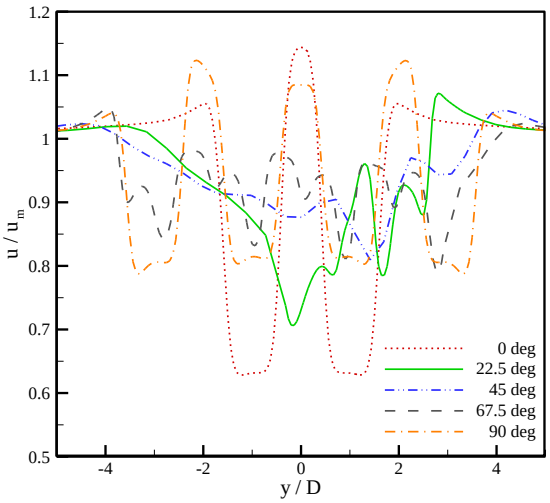

Figure 11. Numerical results of flow velocity along the lateral direction measured at 200 m (5*D*) downstream the center of the fish farm with different incidence angles.

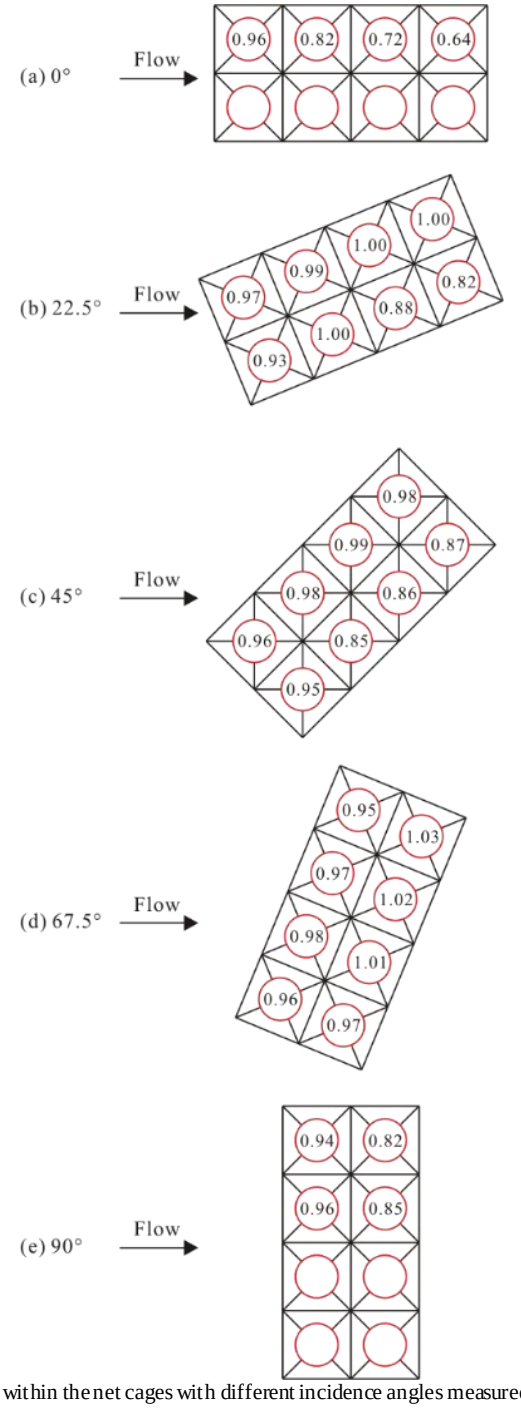

Figure 12. Flow-velocity distribution within the net cages with different incidence angles measured at the cage center.

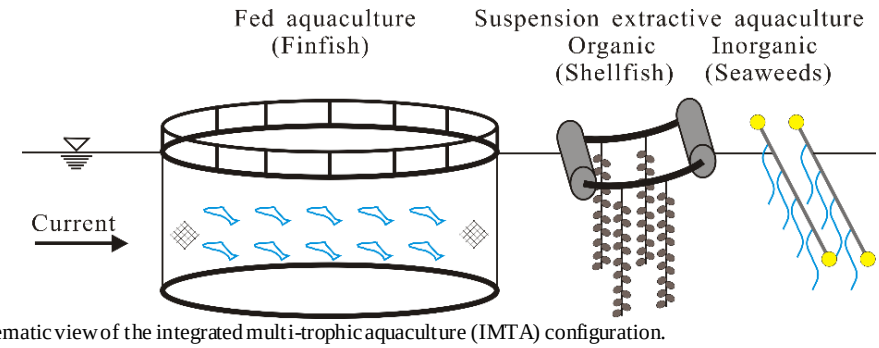

Figure 13. Schematic view of the integrated multi-trophic aquaculture (IMTA) configuration.

followed by diurnal tide, and semi-diurnal tide had the least effect.

(ii) The attenuation in flow velocity both inside the net cage and in the wake region increases as the level of biofouling increases. The maximum attenuation in flow velocity from 51.0% to 70.1% can be found in the vicinity of biofouled net cages compared to 38.3% for the clean net cages.

(iii) For the fish farm oriented at different incidence angles, the staggered net cages are prone to produce more uniformly distributed wake than the tandem net cages. The fish farm at 45°, by contrast, presents the least variation in flow velocity downstream from the net cages. While the fish farm at 67.5° has advantage in providing a uniform flow environment for the caged fish.

The study on flow field in the vicinity region of the fish farm is essential to the analysis of water exchange and nutrient transportation. In addition, the variation in flow velocity should be taken into account in studying the hydrodynamic characteristics of a net cage or cage array; which provides more accurate results for the prediction of the mooring line loads for design of a aquaculture farm. From a wider perspective, the result of this study has implication for the transportation of dissolved nutrients and the hydrodynamic performance of integrated multi-trophic aquaculture (IMTA) configurations.

Acknowledgements

This work was financially supported by the National Natural Science Foundation of China (nos. 51609035 and 51409037) and China Postdoctoral Science Foundation (nos. 2016M590224 and 2017T100176).

Appendix A. The calculation process of the porous coefficients

The drag and lift forces, F_d and F_l, acting on a porous medium can be calculated as follows:

$$\overrightarrow{F_d} = C_n \frac{1}{2}\rho\lambda A\left|\vec{u}\right|\vec{u} \tag{A1}$$

$$\overrightarrow{F_l} = C_t \frac{1}{2}\rho\lambda A\left|\vec{u}\right|\vec{u} \tag{A2}$$

where λ and A are the thickness and area of the porous media, respectively. The drag and lift forces that acts on a plane net can also be calculated from the Morison equation:

$$F_d = \frac{1}{2}\rho C_d A u_0^2 \tag{A3}$$

$$F_l = \frac{1}{2}\rho C_l A u_0^2 \tag{A4}$$

where u_0 is the free stream velocity.

The normal-resistance coefficient C_n is calculated using the least square method by fitting the drag forces of the plane net oriented normal to the current at various flow velocities. The tangential-resistance coefficient C_t is calculated by Morison equation with the empirical formula of lift coefficient proposed by Aarsnes *et al*. (1990):

$$C_l = (0.57S_n - 3.54S_n^2 + 10.1S_n^3)\sin(2\alpha) \tag{A5}$$

where S_n is the net solidity and α is the attack angle that is defined to be the angle between the flow direction and the plane net in the horizontal plane.

Once C_n and C_t are obtained, the normal and tangential resistance coefficients for the plane net at various attack angles can be calculated as follows:

$$C_{n\alpha} = \frac{C_n + C_t}{2} - \frac{C_n - C_t}{2}\cos(2\alpha) \tag{A6}$$

$$C_{t\alpha} = \frac{C_n - C_t}{2}\sin(2\alpha) \tag{A7}$$

References

Aarsnes, J., Rudi, H., & Løland, G. (1990). *Current forces on cage, net deflection.* Paper presented at the Engineering for offshore fish farming. Proceedings of a conference organised by the Institution of Civil Engineers, Glasgow, UK, 17-18 October 1990. Thomas Telford, pp. 137-152.

Bi, C.-w., Zhao, Y.-p., & Dong, G.-h. (2015). Numerical study on the hydrodynamic characteristics of biofouled full-scale net cage. *China Ocean Engineering, 29*(3), 401-414. https://dx.doi.org/10.1007/s13344-015-0028-9

Braithwaite, R. A., Carrascosa, M. C. C., & McEvoy, L. A. (2007). Biofouling of salmon cage netting and the efficacy of a typical copper-based antifoulant. *Aquaculture, 262*(2), 219-226. https://dx.doi.org/10.1016/j.aquaculture.2006.11.027

Chen, H., & Christensen, E. D. (2016). Investigations on the porous resistance coefficients for fishing net structures. *Journal of Fluids & Structures, 65*, 76-107. https://dx.doi.org/10.1016/j.jfluidstructs.2016.05.005

Cornejo, P., Sepúlveda, H. H., Gutiérrez, M. H., & Olivares, G. (2014). Numerical studies on the hydrodynamic effects of a salmon farm in an idealized environment. *Aquaculture, 430*, 195-206. https://dx.doi.org/10.1016/j.aquaculture.2014.04.015

FAO. (2014). *The state of world fisheries and aquaculture*: Food and Agriculture Organization of the United Nations, Rome, Italy.

Fitridge, I., Dempster, T., Guenther, J., & de Nys, R. (2012). The impact and control of biofouling in marine aquaculture: a review. *Biofouling, 28*(7), 649-669. https://dx.doi.org/10.1080/08927014.2012.700478

Gansel, L. C., McClimans, T. A., & Myrhaug, D. (2012). Average flow inside and around fish cages with and without fouling in a uniform flow. *Journal of Offshore Mechanics and Arctic Engineering, 134*(4), 041201.

https://dx.doi.org/10.1115/1.4006150

Gansel, L. C., Plew, D. R., Endresen, P. C., Olsen, A. I., Misimi, E., Guenther, J., & Jensen, Ø. (2015). Drag of Clean and Fouled Net Panels - Measurements and Parameterization of Fouling. *PLoS ONE, 10*(7), e0131051. https://dx.doi.org/10.1371/journal.pone.0131051

Harendza, A., Visscher, J., Gansel, L., & Pettersen, B. R. (2008). *PIV on inclined cylinder shaped fish cages in a current and the resulting flow field.* ASME 2008 27th International Conference on Offshore Mechanics and Arctic Engineering, pp. 555-563.

Johansson, D., Juell, J.-E., Oppedal, F., Stiansen, J.-E., & Ruohonen, K. (2007). The influence of the pycnocline and cage resistance on current flow, oxygen flux and swimming behaviour of Atlantic salmon (Salmo salar L.) in production cages. *Aquaculture, 265*(1-4), 271-287. https://dx.doi.org/10.1016/j.aquaculture.2006.12.047

Johansson, D., Laursen, F., Fernö, A., Fosseidengen, J. E., Klebert, P., Stien, L. H., . . . Oppedal, F. (2014). The interaction between water currents and salmon swimming behaviour in sea cages. *PLoS ONE, 9*(5), e97635. https://dx.doi.org/10.1371/journal.pone.0097635

Klebert, P., Lader, P., Gansel, L., & Oppedal, F. (2013). Hydrodynamic interactions on net panel and aquaculture fish cages: a review. *Ocean Engineering, 58*, 260-274. https://dx.doi.org/10.1016/j.oceaneng.2012.11.006

Kristiansen, T., & Faltinsen, O. M. (2012). Modelling of current loads on aquaculture net cages. *Journal of Fluids and Structures, 34*, 218-235. https://dx.doi.org/10.1016/j.jfluidstructs.2012.04.001

Lader, P., Fredriksson, D. W., Guenther, J., Volent, Z., Blocher, N., Kristiansen, D., & Gansel, L. (2015). Drag on hydroid-fouled nets – An experimental approach. *China Ocean Engineering, 29*(3), 369-389. https://dx.doi.org/10.1007/s13344-015-0026-y

Rasmussen, H. W., Patursson, Ø., & Simonsen, K. (2015). Visualisation of the wake behind fish farming sea cages. *Aquacultural Engineering, 64*, 25-31. https://dx.doi.org/10.1016/j.aquaeng.2014.12.001

Shih, T.-H., Liou, W. W., Shabbir, A., Yang, Z., & Zhu, J. (1995). A new k-ϵ eddy viscosity model for high reynolds number turbulent flows. *Computers & Fluids, 24*(3), 227-238. https://dx.doi.org/10.1016/0045-7930(94)00032-T

Shim, K., Klebert, P., & Fredheim, A. (2009). *Numerical investigation of the flow through and around a net cage.* ASME 2009 28th International Conference on Ocean, Offshore and Arctic Engineering, pp. 581-587.

Swift, M. R., Fredriksson, D. W., Unrein, A., Fullerton, B., Patursson, O., & Baldwin, K. (2006). Drag force acting on biofouled net panels. *Aquacultural Engineering, 35*(3), 292-299. https://dx.doi.org/10.1016/j.aquaeng.2006.03.002

Wu, Y., Chaffey, J., Law, B., Greenberg, D. A., Drozdowski, A., Page, F., & Haigh, S. (2014). A three-dimensional hydrodynamic model for aquaculture: a case study in the Bay of Fundy. *Aquaculture Environment Interactions, 5*, 235-248. https://dx.doi.org/10.3354/aei00108

Xu, T.-J., Hou, H.-M., Dong, G.-H., Zhao, Y.-P., & Guo, W.-J. (2017). Structural Analysis of Float Collar for Metal Fish Cage in Waves. *Turkish Journal of Fisheries and Aquatic Sciences, 17*(2), 257-268. https://dx.doi.org/10.4194/1303-2712-v17_2_04

Zhao, Y.-P., Bi, C.-W., Dong, G.-H., Gui, F.-K., Cui, Y., & Xu, T.-J. (2013). Numerical simulation of the flow field inside and around gravity cages. *Aquacultural Engineering, 52*, 1-13. https://dx.doi.org/10.1016/j.aquaeng.2012.06.001